Available online at www.sciencedirect.com
ScienceDirect
Journal of the European Ceramic Society 27 (2007) 2085–2094
www.elsevier.com/locate/jeurceramsoc

Self-healing mechanisms of a SiC fiber reinforced multi-layered ceramic matrix composite in high pressure steam environments

Ludovic Quemard [a], Francis Rebillat [a,*], Alain Guette [a], Henri Tawil [b], Caroline Louchet-Pouillerie [b]

[a] *Laboratoire des Composites Thermostructuraux, UMR 5801 (CNRS-SAFRAN-CEA-UB1), 3 Allée de la Boétie, 33600 Pessac, France*
[b] *Snecma Propulsion Solide, Les Cinq Chemins, 33187 Le Haillan, France*

Received 5 November 2005; received in revised form 24 June 2006; accepted 30 June 2006
Available online 7 September 2006

Abstract

Non-oxide ceramic matrix composites are potential candidates to replace the current nickel-based alloys for a variety of high temperature applications in the aerospace field. The durability of a $SiC_{(f)}/PyC_{(i)}/[Si,C,B]_{(m)}$ composite with a sequenced self-sealing matrix and Hi-Nicalon fibers was investigated at 600 °C for exposure durations up to 600 h. The specimens are aged in a variety of slow-flowing air/steam gas mixtures and total pressures, ranging from atmospheric pressure with a 10–50% water vapor content to 1 MPa with 10–20% water vapor content. The degradation of the composite was determined from the measurement of residual strength and strain to failure on post-exposure specimens and correlated with microstructural observations, weight changes and characterizations of the generated oxides. All of the post-exposure characterizations demonstrate the ability of the sequenced [Si,C,B] matrix to protect the PyC interphase from environmental attacks. Two different oxidation modes of the matrix, depending on the total pressure are discussed in terms of the reactivity of the boron-containing layers, and their relative positions in the sequenced matrix. In high pressure environments, a strong localized dissolving of a small amount of SiC fibers in the boria-containing oxide is evidenced at 600 °C.

Keywords: SiC; B_4C; Corrosion; Mechanical properties; Lifetime; Engine components

1. Introduction

Non-oxide ceramic matrix composites such as $SiC_{(f)}/PyC_{(i)}/SiC_{(m)}$ consist of SiC matrix reinforced with SiC fibers and Pyrocarbon (PyC) interfacial coating. These composites exhibit a low density associated with high thermomechanical properties and are potential candidates to replace the current nickel-based alloys for a variety of long-term applications in the aerospace field. In these applications, $SiC_{(f)}/PyC_{(i)}/SiC_{(m)}$ components can be subjected to service conditions that include mechanical loading under intermediate to high temperatures and high pressure complex environment containing oxygen and steam. The oxidation of the PyC weak interphase can occur under dry air at a temperature lower than 500 °C and leads to interfacial degradations of $SiC_{(f)}/PyC_{(i)}/SiC_{(m)}$. $SiC_{(f)}/PyC_{(i)}/[Si,C,B]_{(m)}$ composites with a sequenced self-sealing matrix have been developed[1,2] and investigated[3–8,14,15,19] to protect the PyC interphase against oxidation effects up to 1400 °C. The principles of the self-sealing approach are to consume part of the incoming oxygen and limit access of residual oxygen to the PyC interphase by sealing the matrix microcracks with a SiO_2–B_2O_3 oxide phase. However, previous studies showed that B_2O_3[4–6,8,9] and SiO_2[10–13] can volatilize, respectively, at 600 and 1100 °C under water vapor-containing environments. This phenomenon reduces the self-sealing capability, which, in turn, significantly decreases the lifetime of the $SiC_{(f)}/PyC_{(i)}/[Si,C,B]_{(m)}$.

The self-sealing matrix layers are SiC, B_4C and a SiC–B_4C phase noted Si–B–C. At intermediate temperature, the reactivity of crystallized SiC is low and the self-sealing process involves the B_4C and Si–B–C layers. The efficiency of the self-sealing process under environments containing both oxygen and water vapor results from the competition between the oxidation of these matrix layers and the volatilization of the resulting oxide phase.

* Corresponding author. Fax: +33 5 56 84 12 25.
E-mail address: rebillat@lcts.u-bordeaux1.fr (F. Rebillat).

0955-2219/$ – see front matter © 2006 Elsevier Ltd. All rights reserved.
doi:10.1016/j.jeurceramsoc.2006.06.007

Under dry air, B_4C undergoes oxidation and volatilization reactions, respectively, below 600 and 900 °C, as shown below[4–6,8,9]:

$$B_4C_{(s)} + 4O_{2(g)} \rightarrow 2B_2O_{3(l)} + CO_{2(g)} \quad (1)$$

$$B_2O_{3(l)} \rightarrow B_2O_{3(g)} \quad (2)$$

Under water vapor-containing environments, $B_2O_{3(l)}$ may react significantly at 600 °C to form hydroxydes by the following reactions[4–6,8,9]:

$$\frac{3}{2}B_2O_{3(l)} + \frac{3}{2}H_2O_{(g)} \rightarrow H_3B_3O_{6(g)} \quad (3)$$

$$\frac{3}{2}B_2O_{3(l)} + \frac{1}{2}H_2O_{(g)} \rightarrow H_3BO_{3(g)} \quad (4)$$

$$\frac{1}{2}B_2O_{3(l)} + \frac{1}{2}H_2O_{(g)} \rightarrow HBO_{2(g)} \quad (5)$$

The competition between the oxidation (1) and volatilization reactions ((2)–(5)) can result in a continuous consumption of B_4C, also called recession. The Si–B–C matrix layer can be described as a mixture of SiC nanocrystals in an amorphous B_4C phase.[7] A previous study investigated the oxidation of Si–B–C coatings under oxygen and steam-containing-environments by thermogravimetric analysis.[4,5] It has been shown that SiC nanocrystals can oxidize significantly at 600 °C and at atmospheric pressure to form silica according to the following reaction:

$$2SiC_{(s)} + 3O_{2(g)} \rightarrow 2SiO_{2(s)} + 2CO_{(g)} \quad (6)$$

The aim of this study is to evaluate the effects of both oxygen and water wapor on the self-sealing process of $SiC_{(f)}/PyC_{(i)}/[Si,C,B]_{(m)}$ composites, subjected to high pressure-steam environments at intermediate temperature. Corrosion tests were conducted for different periods of time on $SiC_{(f)}/PyC_{(i)}/[Si,C,B]_{(m)}$ specimens at 600 °C in oxygen and steam-containing-environment at atmospheric pressure and high pressure. Post-exposure mechanical tests were performed at room temperature to investigate the effects of corrosion on the ultimate tensile properties. Corrosion tests were also conducted on B_4C and Si–B–C coatings for comparison purposes.

2. Materials and test specimens

The material investigated is the CERASEP® A410[14,15] (noted C410) manufactured by Snecma Propulsion Solide (France) via Chemical Vapor Infiltration (CVI). It is a woven-Hi-Nicalon® SiC-fiber reinforced [Si,C,B] sequenced matrix composite (Fig. 1). The different matrix layers are crystallized SiC, amorphous B_4C and a SiC–B_4C phase named Si–B–C which can be described as a mixture of SiC nanocrystals in a B_4C amorphous phase. Fiber volume fraction, material density and mainly closed bulk porosity, as reported by the composite manufacturer, are respectively, 34%, 2.25 ± 0.05 and 13 ± 1%. The interphase is PyC.

The test specimen geometry used in this study has a reduced gauge section (Fig. 2). It is 200 mm long, with a grip section width of 24 mm, a reduced gauge section width of 16 mm, and a thickness of 4.4 mm. The dog-bone specimens are machined

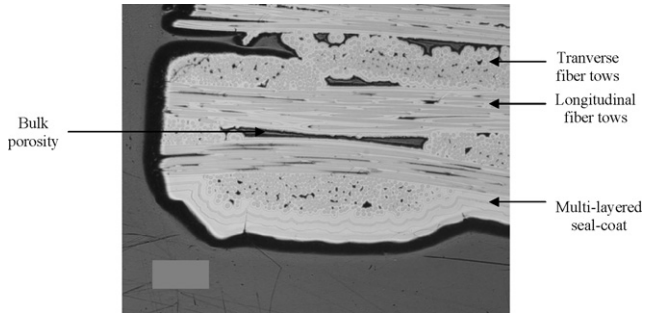

Fig. 1. Polished cross-section of the as-received C410 material.

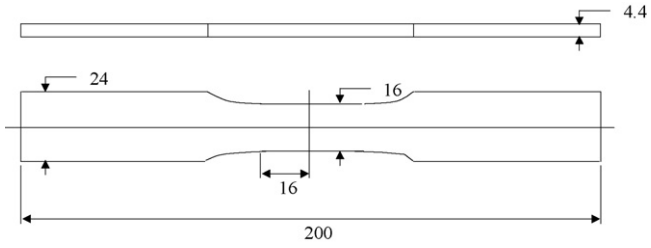

Fig. 2. C410 specimen geometry used in this study. Dimensions are in millimeters.

from composite plates using diamond grinding and then are seal-coated with CVI layers of SiC, B_4C and Si–B–C. The sequenced seal-coat thickness, with a SiC final layer, is 120 μm on the composite surface and about 40 μm on the machined edges. Corrosion tests are also performed on Si–B–C and B_4C coatings for comparison purposes. The coatings, with a thickness of 30 ± 3 and 50 ± 5 μm, respectively, are deposited on SiC chips (diameter of 8 mm and thickness of 2 mm) via Chemical Vapor Deposition (CVD).

3. Test procedures

3.1. Pre-damaging

The dog-bone specimens are loaded in tension monotonically at room temperature (RT) to a tensile stress of 150 MPa (the stress corresponding to twice their elastic limit) then unloaded before the exposures. The aim of this pre-damaging is to generate a controlled crack network in the matrix, thus facilitating the ingress of the corrosive species. The residual strain is very low (≅0.001 %) and can be neglected for post-exposure mechanical tests. The pre-damaging microcracks are mainly located in the seal-coat of the gauge section of the specimens (Fig. 3). At RT, their mean spacing distance is 230 ± 30 μm and their width is 0.5–3 μm. In addition, few microcracks with a width lower than 1 μm at RT are present at the edge of the porosities.

3.2. Corrosion tests

The corrosion test conditions are reported in Table 1. Two corrosion test equipments are used for these tests. High pressure corrosion tests are conducted in the High Pressure–High Temperature Furnace[16] (Fig. 4). High pressure air is provided

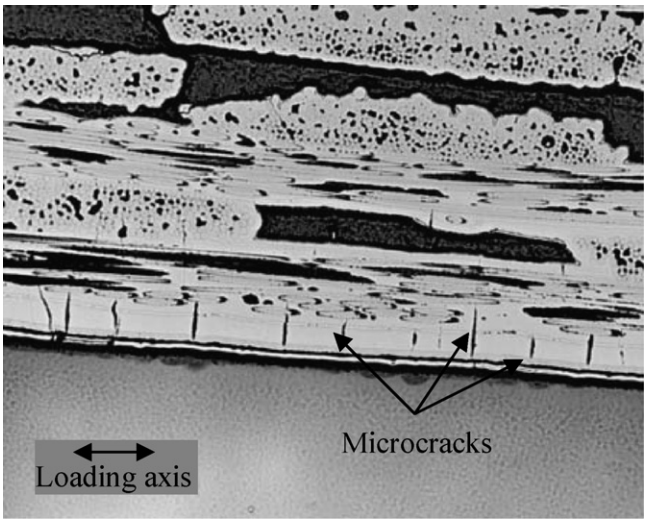

Fig. 3. Polished cross-section of the gauge section of a C410 specimen pre-damaged in tension (150 MPa) at RT.

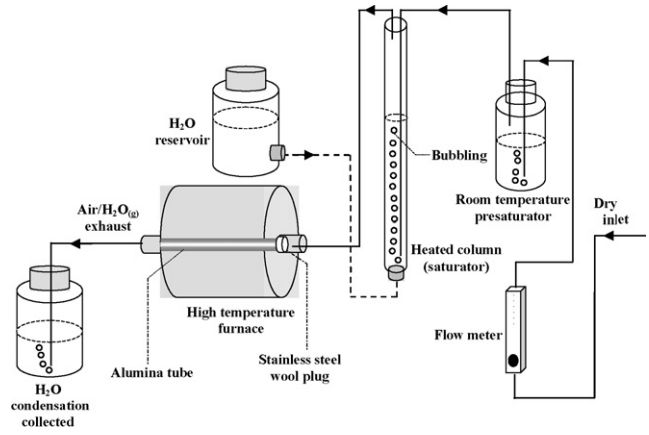

Fig. 5. Schematic of the high temperature furnace and the water vapor saturator at atmospheric pressure.

by a pressurized gas supply system then mixed with water in an evaporator. The air and water flows are independently controlled by mass flow meters and the air/H_2O gas mixture is injected in the alumina test tube (inner diameter: 34 mm, purity: 99.7 %, OMG, France) of the furnace. A system of pneumatically driven back pressure reducers maintains a slight difference of pressure between the tube interior and the metallic vessel ($P_{tube} - P_{vessel} = -3$ kPa). This makes it possible to minimize stresses on the tube and increase its airtightness. The uniform heating zone of the furnace is approximately 120 mm long which is longer than the gage length of the dog-bone specimens.

A high temperature furnace associated with a water saturator is used to run the corrosion tests at atmospheric pressure (Fig. 5). The dry air flows through a heated water column in order to be saturated in steam before its introduction in the alumina tube (inner diameter: 34 mm, purity: 99.7%, OMG, France) of the furnace. The temperature of the water in the column is slightly higher than the dewpoint corresponding to the desired water vapor partial pressure. For example, an air/steam (90/10) gas

Table 1
Summary of test conditions for C410 specimens exposed at 600 °C in various environments.

No.	Exposure	T (°C)	P_{tot} (MPa)	Air/steam	P_{O_2} (kPa)	P_{H_2O} (kPa)	P_{H_2O}/P_{O_2}	v (cm s^{-1})
A	Furnace	610 ± 10	0.1	90/10	18	10	0.56	5
B	Furnace	600 ± 10	0.1	50/50	10	50	5	10
C	HP Furnace	625 ± 20	0.45	90/10	81	45	0.56	8
D	HP Furnace	620 ± 30	1	90/10	180	100	0.56	8
E	HP Furnace	620 ± 30	1	80/20	160	200	1.25	8

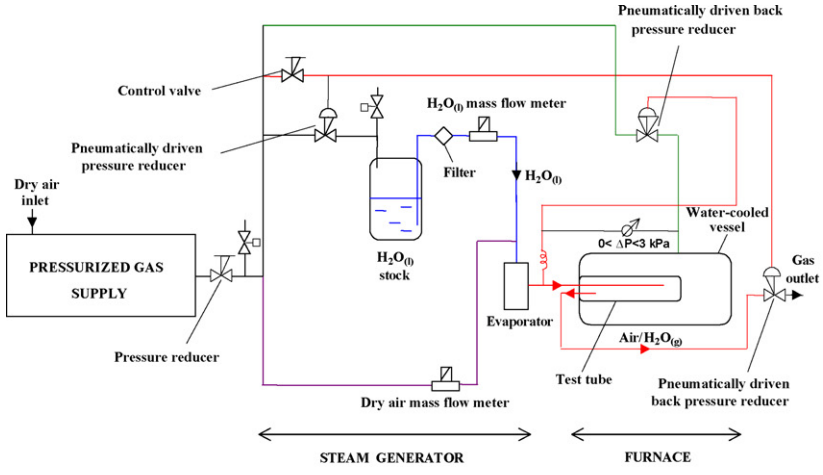

(a)

(b)

Fig. 4. Schematic of the high temperature–high pressure corrosion test equipment (a), and view of the furnace (b).

mixture is obtained for a column temperature of 48 °C (dewpoint for $P_{H_2O} = 10$ kPa is 46 °C). Water content in the gas stream is monitored by measuring the condensate in the gas exhaust daily and the amount of water in the stock which supplies the heated column. The uniform heating zone of the furnace is approximately 220 mm long.

In both corrosion test equipments, the C410 specimens are oriented parallel to the gas flow and placed on alumina sample holders (purity: 99.7%, OMG, France) specially designed. The heating and cooling rates, used at atmospheric pressure under ambient air, are respectively, 150 and 100 °C h^{-1}. The exposures are regularly interrupted to weigh the specimens using a scale (Precisa Instruments AG, Switzerland) with an accuracy of 1×10^{-2} mg.

3.3. Characterization of specimens after exposure

Post-exposure cyclic tensile tests are performed at RT on the dog-bone specimens. A spring-loaded clip on-gauge is attached to the 25 mm length of the straight section of the samples to record displacement. The composites are tested up to failure in a servo controlled testing machine (INSTRON 1185) equipped with self-aligning grips at a deformation speed of $0.40 \pm 0.05\%$ min^{-1}.

After exposures, the test specimens are cut perpendicularly and parallel to the loading axis then polished for examination using an optical microscope. Moreover, the fractured surfaces are analyzed by Scanning Electron Microscopy (SEM). The oxide scales, formed at the surfaces of the composites, are characterized by Raman microspectrometry (Labram 10 spectrometer from Jobin Yvon, France) and infra-red spectroscopy (Bruker IFS66). X-ray photoelectron spectroscopy (ESCALAB VG 220i-XL) is used to evaluate the composition of the oxide scales at the surface of the exposed B_4C and Si–B–C coatings.

4. Results

4.1. Post-exposure mechanical results

The post-exposure mechanical properties of the C410 pre-damaged specimens are determined using tensile tests at RT. The results are shown in Fig. 6 and reported in Table 2. Cyclic tensile tests were performed on all samples except for the one aged at atmospheric pressure in an air/steam mixture (50/50) which was tested monotonically. Three C410 samples were used to determine the mechanical properties of the as-received material at room temperature. The retained mechanical properties of all the exposed composites show no significant changes, by comparison with the C410 database[14,15] and the as-received material (Fig. 6 and Table 2).

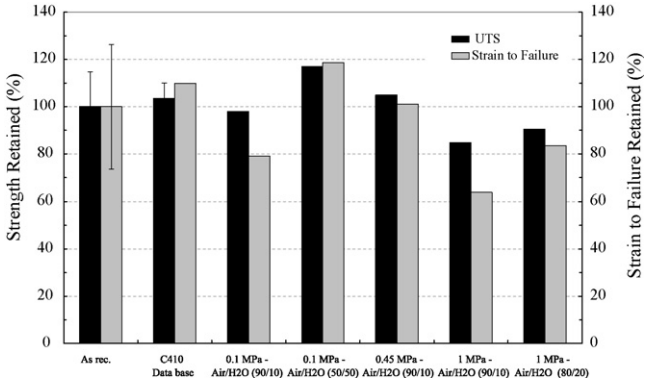

Fig. 6. Effect of corrosion environments on the UTS and the strain to failure of the C410 material.

Fig. 7. SEM representative fracture surface of a non-brittle rupture on the C410 specimen exposed for 611 h at 600 °C and 1 MPa in an air/steam (80/20) gas mixture.

All the samples have gage failures with a non-brittle rupture characterized by fiber pull-out (Fig. 7). The exposed composites and the as-received materials have a similar mechanical behavior (Fig. 8). Thus, a non-linear stress–strain behavior without a plateau is observed up to the ultimate rupture of the specimens.

Table 2
Summary of C410 specimen post-exposure tensile properties at RT

Test condition	Exposure time (h)	Weight change (%)	Tensile test	UTS (MPa)	Strain to failure (%)	E (GPa)
A	606	−0.55	Cyclic	298	0.36	290
B	600	+0.11	Monotonic	356	0.54	280
C	603	−1.01	Cyclic	319	0.46	250
D	562	+0.16	Cyclic	258	0.29	164
E	611	+0.33	Cyclic	275	0.38	210
As rec.[a]	–	–	Cyclic	304 ± 45	0.46 ± 0.12	252 ± 4
C410 database[14,15]	–	–	M.&C.	315 ± 20	0.5	220 ± 25

[a] Three samples tested.

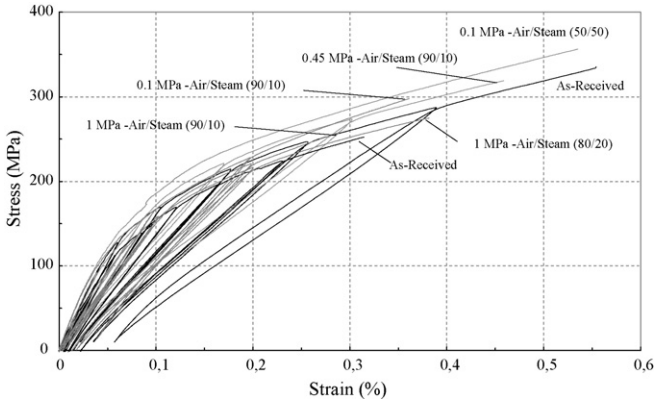

Fig. 8. Stress–strain curves of the C410 composites obtained at RT after exposure for 600 h at 600 °C in various environments.

This behavior, induced by matrix cracking, indicates a progressive damaging. Moreover, the width of the hysteresis loops is narrow and the residual strains after unloading are very low. This indicates a high fiber-matrix load transfer, thus a strong interfacial shear stress. The variation of the elastic modulus is measured, from the stress–strain curves, at each of the load-unload loops to highlight the damage progression in the material (Fig. 9). First, the initial modulus of the aged composites has to be compared with the as-received material modulus corresponding to the stress used for the pre-damaging (150 MPa). Thus, the exposed materials have an initial modulus similar to or higher than the modulus of the as-received material corresponding to a stress of 150 MPa. This is consistent with the sealing of the pre-damaging cracks with an oxide phase which is solid at RT. Fig. 9 shows a similar damage progression mode, in the exposed specimens and in the as-received composites. The modulus values at failure, determined using a linear extrapolation of the measured modulus (dotted lines in Fig. 9), are compared with the theoretical modulus at failure E_{Th}. It is calculated from the following relation:

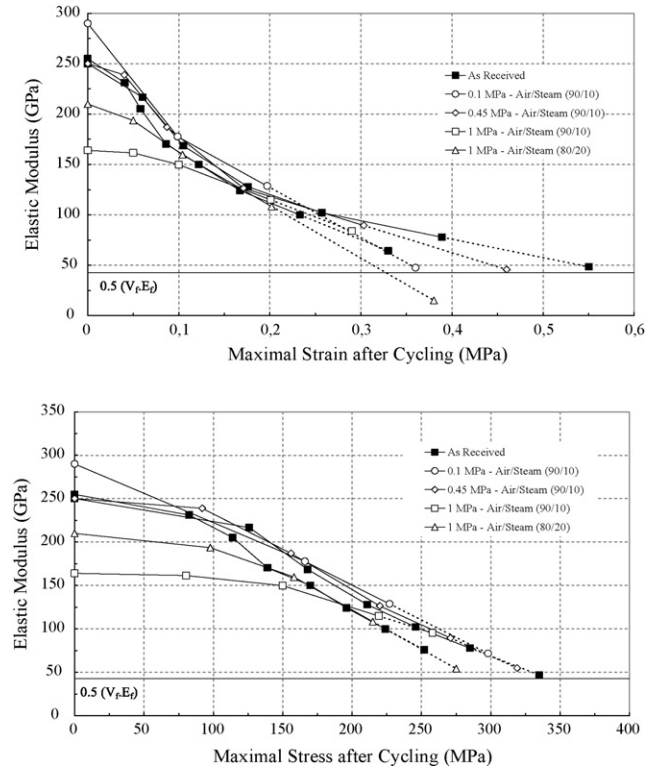

Fig. 9. Damage progression of C410 specimens during tensile cycling at RT after exposures at 600 °C for 600 h in various environments. (The dotted lines correspond to the modulus at failure extrapolated from (7).)

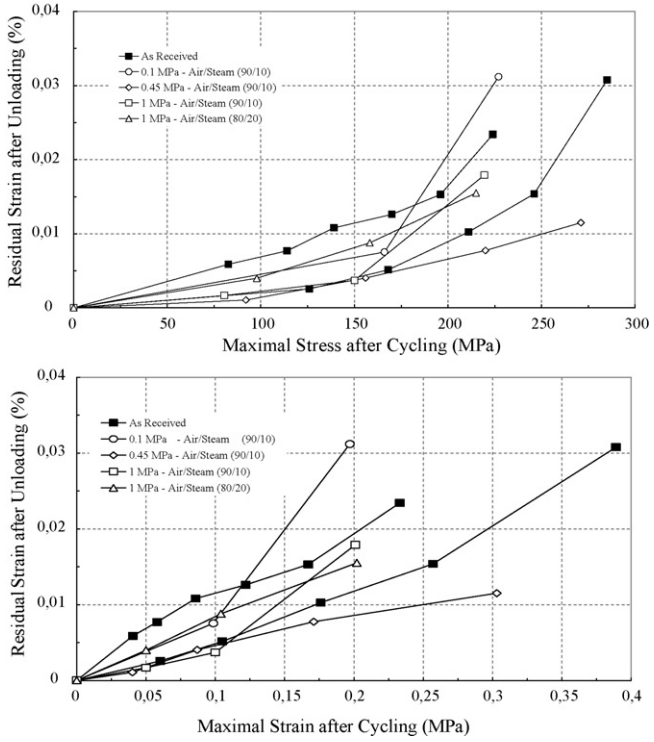

Fig. 10. Variation of the residual strains after unloading of C410 specimens during tensile cycling at RT after exposures at 600 °C for 600 h in various environments.

$$E_{Th} = \frac{1}{2} \times V_f \times E_f \quad (7)$$

where V_f is the fiber volume (34%), E_f the fiber modulus at RT (Hi-Nicalon® Fiber: 250 GPa) and E_{Th} is the theoretical modulus at failure of a 2D woven composite considering that only the fibers oriented in the direction of the loading axis bear the load at failure.

Most of the extrapolated modulus values at failure of the exposed specimens and the as-received composites are similar to E_{Th}, which confirms an un-changed damage progression mode (Fig. 9). The residual strains, measured after unloading at each loop, are shown in Fig. 10. The variations of the residual strains of the aged materials are similar to those of the as-received samples. This indicates that exposures for 600 h at 600 °C do not affect significantly the fiber-matrix bond[17,18] of the composites. All of the post-exposure mechanical results show that the [Si,C,B] matrix could provide protection to the PyC interphase in the environments tested.

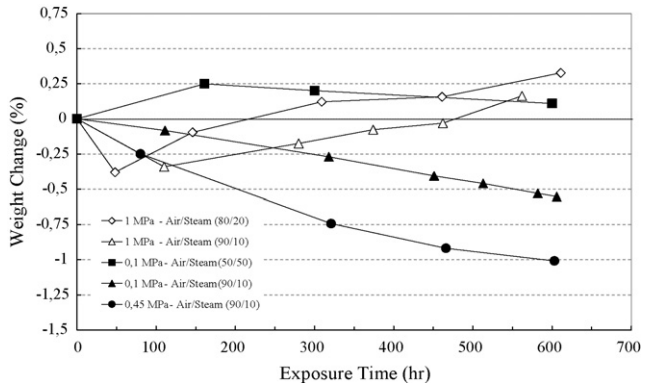

Fig. 11. Weight changes of C410 specimens exposed in various environments at 600 °C up to 600 h.

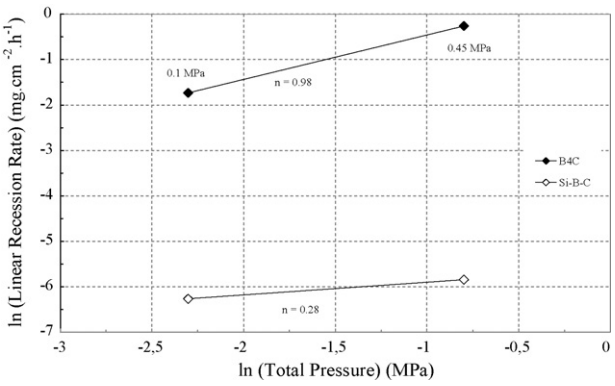

Fig. 13. Linear recession rates of B_4C and Si–B–C coatings exposed up to 600 h in the air/steam (90/10) gas mixture at 600 °C. Estimation of the order "*n*" associated with the total pressure.

4.2. Weight changes

The weight changes of C410 specimens exposed in various environments up to 600 h are reported in Table 2 and shown in Fig. 11. The weight changes are low, between −1 and +0.33%, and could be related to limited corrosion phenomena. Nevertheless, two different behaviors are observed. Indeed, the materials tested at high steam pressure present, after a short transition period (weight loss), a weight gain rate (positive slope) while the composites, aged at 0.45 and 0.1 MPa show linear weight loss rates (negative slope).

The weight changes of the B_4C and Si–B–C coatings in various environments up to 600 h are given in Fig. 12. B_4C and Si–B–C coatings show linear weight losses, characteristic of recession phenomena. According to the generation of silica, the linear recession rates of Si–B–C coatings, in an air/steam (90/10) gas mixture flowing at 0.1 and 0.45 MPa, are 100–250 times lower than for B_4C (Fig. 12). The B_4C recession rate at 0.45 MPa is minimized. Indeed, the determination of the B_4C coating recession rate requires short tests, due to its high reactivity and its low thickness. However, the HT-HP furnace is not well-adapted to perform corrosion tests under 15–20 h. Increasing the total pressure by a factor 4.5 enhances the recession rates of Si–B–C and B_4C, respectively, by a factor 1.5 and at least 4.5 (Fig. 12). In agreement with the generation of silica, the recession rate of the Si–B–C is dependent to the total pressure with an order at least 3.5 times lower than the B_4C coating one (Fig. 13). The Si–B–C coating, aged at 1 MPa air/steam (80/20), shows a high and non-linear recession rate. This is consistent with the enhancement of the oxidation and volatilization processes due to the high P_{O_2} and P_{H_2O}.

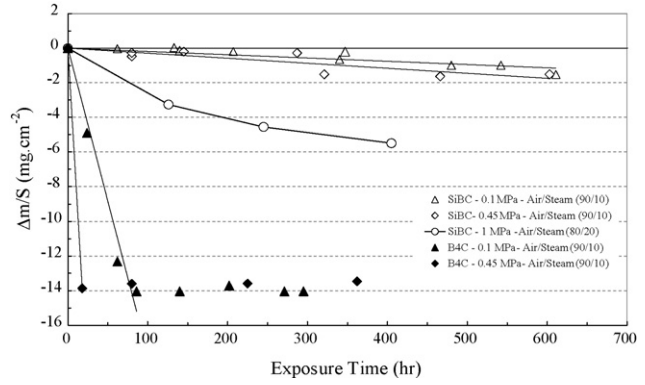

Fig. 12. Weight changes of B_4C and Si–B–C coatings exposed up to 600 h in various environments at 600 °C.

4.3. Post-exposure observations of C410 specimens

Fig. 14 highlights the oxidation of the boron-containing matrix layers which is responsible for the weight gain rate of specimens exposed at 1 MPa. This oxidation occurs through the pre-damaging cracks located in the seal-coat and in the matrix,

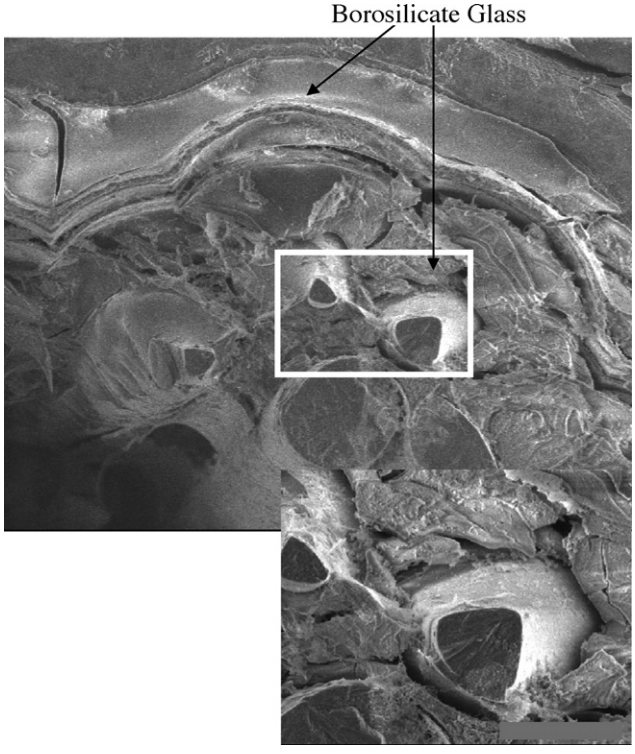

Fig. 14. SEM fracture surface of a C410 specimen exposed at 600 °C and 1 MPa in an air/steam (80/20) gas mixture for 611 h, showing the oxidation of the boron-containing matrix layers and the dissolving of the SiC fibers at the tip of the pre-damaging cracks.

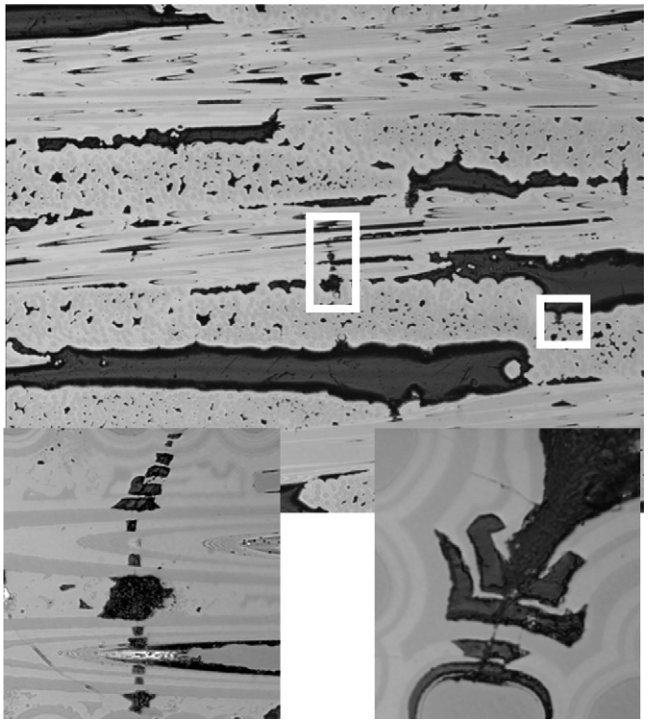

Fig. 15. Polished cross section of a C410 specimen, exposed at 600 °C and 0.45 MPa in an air/steam (90/10) gas mixture for 603 h then tested in tension at RT, showing the recession of the boron-containing matrix layers in pre-damaging cracks and the initiation of the dissolving of a SiC fiber.

at the edge of the bulk porosities. Only the fibers located at the tip of the pre-damaging cracks have a local reduction of their section (up to 75% after 600 h). This is due to the localized dissolving of SiC fibers in the boria-containing oxide, flowing from the oxidized layers through the matrix pre-damaging cracks, in agreement with the following reaction[19–21]:

$$x\mathrm{SiC}_{(s)} + y\mathrm{B_2O_{3(l)}} = z\mathrm{B_2O_3} - v\mathrm{SiO_{2(sou l)}} + u\mathrm{CO_{(g)}} \quad (8)$$

However, only a low amount of fibers is attacked (Fig. 7) and the fiber-matrix load transfer of the exposed composite is not significantly affected (Figs. 6 and 10).

A cross section from the gauge region of a C410 specimen aged for 603 h at 600 °C and 0.45 MPa in an air/steam (90/10) gas mixture is shown in Fig. 15. The composite weight loss (−1.01%) is due to the boron-containing matrix layers recession through the pre-damaging cracks located in the seal-coat and in the tows (Fig. 15). Nevertheless, the initiation of the dissolving of the SiC fiber highlights the sealing of the cracks by a boria-containing oxide (Fig. 15). Similar analyses and conclusions were obtained on the materials aged at atmospheric pressure. The amount of fibers attacked is lower than for the samples exposed at 1 MPa and does not affect the fiber-matrix load transfer (Fig. 7) and the retained mechanical properties of the composite (Fig. 6).

4.4. Characterization of the oxide scales

Raman microspectrometry (RMS) analyses were carried out on the external surface of the C410 materials aged in various environments, without any specific preparation. Raman spectra, recorded from an oxide drop adjacent to a pre-damaging crack of a composite exposed for 309 h at 1 MPa in an air/steam (80/20) gas mixture show only 2 sharp peaks at 808 and 882 cm^{-1}. They are characteristic of the B_2O_3 (boroxol rings) and H_3BO_3 ($1/2\ B_2O_3 - 3/2\ H_2O$) phases. Similar spectra were obtained for many conditions as soon as oxide drops were present after exposure.

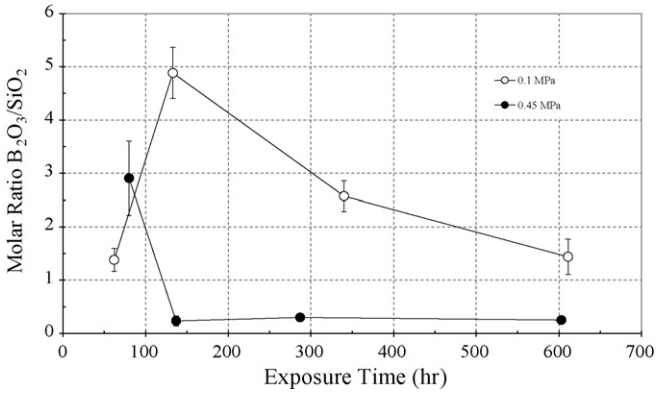

Fig. 16. Mean composition of the oxide scales formed at the surface of Si–B–C coatings exposed at 600 °C in the air/steam (90/10) gas mixture up to 600 h. Results obtained using XPS analysis.

Taking into account that amorphous silica cannot be detected with RMS, the oxide scales were also analysed by infra-red spectroscopy (IRS). Thus, IRS spectra, recorded from oxide drops taken from the surface of a composite exposed at 0.45 MPa for 462 h in an air/steam (90/10) gas mixture present 5 bands, characteristic of B–O bonds, at 3220, 1472, 1196, 784 and 548 cm^{-1} but no bands corresponding to the Si–O or Si–O–B bonds. This is consistent with the RMS results and indicates that the oxide drops are pure boria or borosilicate glasses rich in boria and confirms the filling of the pre-damaging cracks by a glass generated from the oxidation of the boron-containing matrix layers.

In addition, X-ray photoelectron spectroscopy (XPS) analyses were carried out on the borosilicate scales formed at the surface of the Si–B–C coatings exposed at 0.1 and 0.45 MPa in the air/steam (90/10) gas mixture (Figs. 16 and 17). The results, in Fig. 16, are obtained from line scanning at different locations

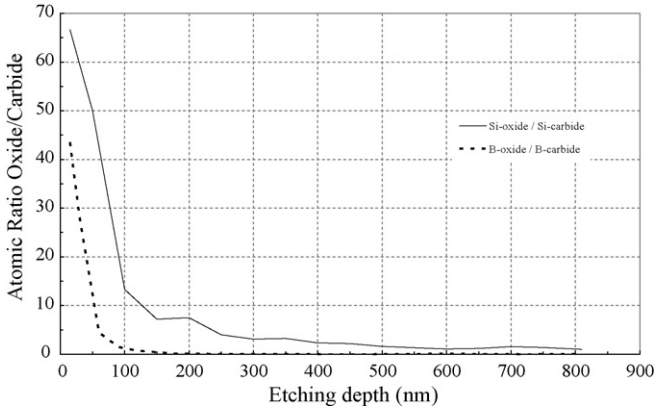

Fig. 17. Comparison of the oxidation levels of SiC and B_4C phases in a Si–B–C coating exposed for 287 h at 600 °C and 0.45 MPa in the air/steam (90/10) gas mixture. Results obtained using XPS analyses.

on the surface. Previously to these analyses, an etching time of 60–120 s was used to eliminate the carbon pollution. At atmospheric pressure, the boria content increases up to 130 h then diminishes continuously up to 600 h (Fig. 16). The decrease of the boria content is due to its high volatility in steam environment which causes the Si–B–C coating to loose weight (Fig. 12). The increase of the boria content, up to 130 h, would be due to the competition of SiC nano-crystals and B_4C major phase oxidation kinetics. Indeed, Fig. 17 shows that a significant amount of silica is detected deep inside the B_4C major phase, indicating that the SiC nano-crystals oxidation rate is higher than the B_4C matrix one at 600 °C. Thus, initially, the oxide scale has a high silica content, then becomes more and more rich in boria, due to the oxidation of the B_4C major phase. The boria content is limited by its volatility in steam environments and the increase of the amount of silica. Thus, the boria content begins to decrease after 130 h. At high pressure, the dramatic decrease of the boria content after only 80 h is due to the acceleration of the oxidation and volatilization rates. This is consistent with the increase of the recession rates in high pressure environments, caused by the high P_{O_2} and P_{H_2O} (Fig. 13).

5. Discussion

5.1. Durability of the CERASEP®A410

The post-exposure mechanical results, determined at room temperature, show that all the corrosion tests at 600 °C do not affect the C410 material mechanical behavior (UTS, strain to failure, damage progression). According to these results, the C410 weight changes are low and the morphological examinations show no major degradation of the fiber reinforcement and the fiber-matrix bond. Thus, at low pressure, the recession of the boron matrix layers occurs but the sealing, close to the fibers located at the tip of the pre-damaging cracks, protects the major part of the tows from oxidation. In high pressure environments, the pre-damaging cracks are sealed by oxidation of all the boron-containing matrix layers. However, a small amount of fibers, located at the tip of the pre-damaging cracks are severely attacked by the boria-containing oxide which flows through the cracks. Nevertheless, all of the post-exposure characterizations demonstrate the ability of the sequenced [Si,C,B] matrix to protect the PyC interphase at 600 °C for exposures up to 600 h.

Those results are in agreement with recent studies[3,22,23] conducted at Pratt and Whitney (Florida, USA) and at Arnold Engineering Development Center (AEDC, Arnold Air Force Base, Tennessee, USA). These works consisted in testing C410 seals in Pratt and Whitney engines that power the F-16 and F-15 fighters. The seals were tested in ground engines for nearly 1300 h including 100 h in afterburner conditions, that corresponds to a number of Total Accumulated Cycles (TAC) of 5000 approximately. The maximal stresses in the seals, calculated taking into account the worst-case flight point corresponding to the after burner conditions, were 63 MPa (760 °C) in the 1–1 axis (exit end) and 55 MPa (430 °C) in the 2–2 axis (forward hinge). The post-exposure mechanical results showed no decrease of the ultimate tensile properties at RT.

5.2. Effect of the total pressure

The weight changes and the morphological analyses highlight effects of the total pressure. Thus, composite weight gain rates are obtained at 1 MPa while weight loss rates are obtained

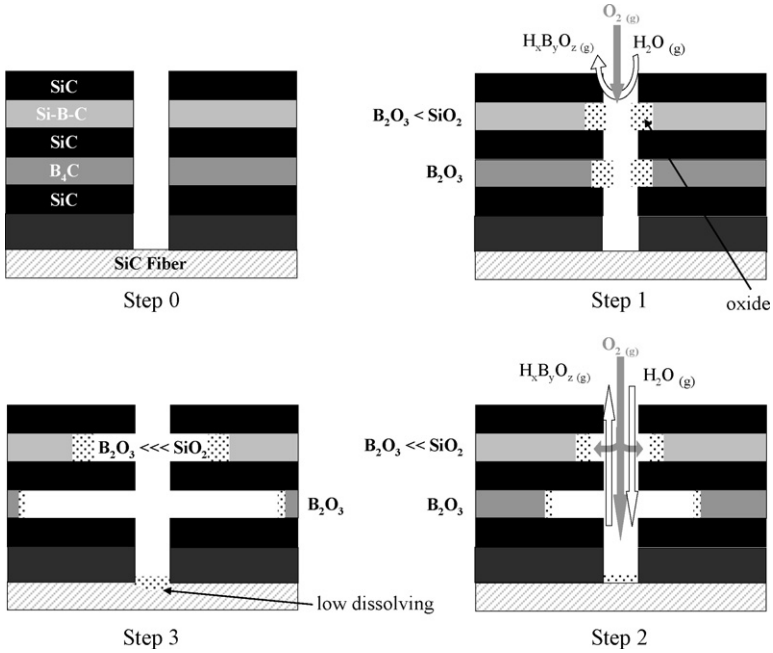

Fig. 18. Proposed degradation process of the [Si,C,B] matrix at 600 °C and 0.1 MPa in air/steam (90/10) and (50/50) gas mixtures, and at 0.45 MPa in an air/steam (90/10) gas mixture, showing the recession of the boron-containing layers and the sealing of the inner boron-containing layers (layers not represented).

in lower pressure environments (Fig. 11). These weight changes are essentially due to the boron matrix layers recession and oxidation processes. Indeed, the SiC fibers and the SiC matrix layers are assumed to be relatively inert to oxygen and steam at 600 °C. Also, considering the low amount of PyC in the composite, its oxidation cannot affect the weight changes. According to the post-exposure observations and the weight changes of the C410 composites and the boron coatings, the weight loss rates at atmospheric pressure and at 0.45 MPa result from the recession of a part of the boron matrix layers which is due to a competition between the kinetics of oxidation and volatilzation (1, 3, 4, 5 and 6).

A scenario of the corrosion progression through a pre-damaging crack in the [Si,C,B] matrix is depicted in Fig. 18. It leads to a weight loss and a low dissolving of the fiber in the borosilicate glass generated by oxidation of the boron-containing layers located near the crack tip (Fig. 18, step 3). This sealing, close to the fiber, is made possible by the decrease of P_{H_2O} through the crack, since water vapor reacts with glass (Fig. 18, step 2). At the opposite, the weight gain rates (positive slopes) obtained at 1 MPa result from a boron matrix layers oxidation higher than the boria volatilization (Fig. 11). Taking into account the significant weight loss of the Si–B–C coating aged at 1 MPa (Fig. 12), the C410 weight gain rates may be explained by the particular position of the boron matrix layers (Fig. 19). Indeed, at 600 °C, the Si–B–C layer, placed above the B_4C layer, is the first boron component in contact with the environment, through a reduced space (crack). Thus, at 1 MPa, the high Si–B–C oxidation rate makes possible the quick filling of the pre-damaging crack with a borosilicate glass. This transition period is characterized by an initial weight loss rate of the composite due to the simultaneous volatilization of the generated boria (Fig. 11 and Fig. 19, step 1). The sealing borosilicate reacts with water vapor, thus increasing the silica content on its outer surface and reducing significantly the water vapor diffusion to the boria generated by the B_4C layer oxidation (Fig. 19, step 2). Simultaneously, part of the oxygen continues to diffuse toward the B_4C layer and causes the amount of boria to increase (Fig. 19, step 3). This phenomenon results in a weight gain rate of the C410 material (Fig. 11) and the local dissolving of a small amount of SiC fibers, located at the crack tips, in the boria-containing glass (Fig. 19, step 3).

5.3. Dissolving of the SiC fibers at intermediate temperature

Previous studies[19–21] on the durability of Hi-Nicalon®/BN/SiC composites have shown that the dissolving of the fibers in boria generated by the interphase oxidation, occurs in a high velocity burner rig (Mach 0.3) after 150 h at 800 °C and 0.1 MPa. Only the edge of the fibers is attacked but they are strongly bridged together with silica and the retained mechanical properties are dramatically reduced. The degradation is enhanced by the oxidation of a continuous carbon-rich layer on the as-produced surface of the Hi-Nicalon® fibers. In the C410 material exposed in high pressure environments, the amount of attacked fibers is much lower than for the Hi-Nicalon®/BN/SiC (its retained mechanical properties are maintained) but the dissolving severely reduced the fiber section (up to 75% after 600 h). Assuming that the dissolving rate is lower at 600 °C than at 800 °C, the strong section reduction is due to the amount of boria in contact with fibers and to the exposure time which are both greater than for the Hi-Nicalon®/BN/SiC.

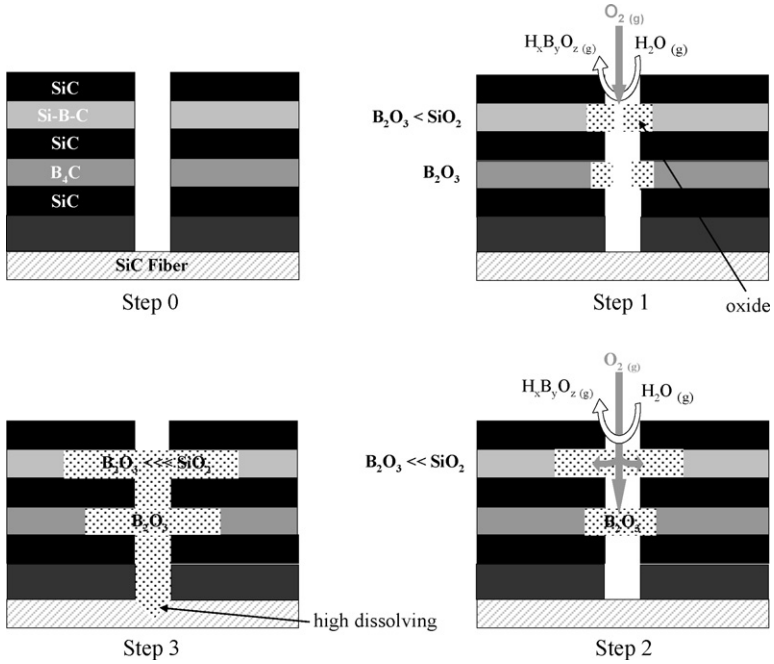

Fig. 19. Proposed oxidation process of the [Si,C,B] at 600 °C and 1 MPa in air/steam (90/10) and (80/20) gas mixtures, showing the sealing of the inner boron-containing layers and the high dissolving of SiC fibers.

6. Conclusions

The study of $SiC_{(f)}$/ $PyC_{(i)}$/$[Si,C,B]_{(m)}$ specimens exposed for periods up to 600 h at 600 °C in slow-flowing air–steam gas mixtures, in an atmospheric pressure furnace and in a high-pressure furnace, have shown several results. All of the post-exposure characterizations performed on C410 pre-damaged composites indicate that the PyC interphase can be protected by the sequenced [Si,C,B] matrix from environmental attacks. Indeed, the corrosion-resistance capability of the material is maintained after exposures for 600 h. At 600 °C, the sealing ability of the C410 material involves the boron matrix layers but increasing the total pressure affects the matrix oxidation rate. Thus, at a low pressure, the limitation of the diffusion of O_2 and $H_2O_{(g)}$ through the pre-damaging cracks, is related to the consumption of the boron matrix layers (recession) and to the filling of the cracks, close to the fiber. In high pressure environments (1 MPa), the high oxidation rate of all the boron-containing layers, due to high P_{O_2} and to the relative positions of the boron-containing layers in the matrix, makes possible to fill quickly the pre-damaging cracks. However, a strong localized dissolving of a small amount of fibers occurs in the boria-containing glass which flows through the pre-damaging cracks.

Acknowledgements

This work has been supported by the Centre National de la Recherche Scientifique (CNRS) and Snecma Propulsion Solide (SPS) through a grant given to L. Quémard. The authors are grateful to M. Cataldi, J. Lamon and G. Falguieres for fruitful discussions, Snecma for production of the samples, R. Bouvier for assistance with corrosion tests, P. Ophele and F. Labarriere for assistance with mechanical tests and C. Labrugere for assistance with XPS analyses.

References

1. Lamouroux, F., Pailler, R., Naslain, R. and Cataldi, M., French Patent no. 95 14843, 1995.
2. Vandenbulcke, L. and Goujard, S., Multilayer systems based on B, B_4C, SiC and SiBC for environmental composite protection. *Prog. Adv. Mater. Mech.*, 1996, 1198–1203.
3. Bouillon, E., Spriet, P., Habarou, G., Louchet, C., Arnold, T. and Ojard, G. C. *et al.*, Engine Test and Post Engine Test Characterization of Self Sealing Ceramic Matrix Composites for Nozzle Applications in Gas Turbine Engines, *ASME TURBO EXPO 2004, Power for Land, Sea and Air*, Vienna, Austria, 2004, ID GT-2004-53976.
4. Martin, X., Rebillat, F. and Guette, A., Oxidation behavior of a multilayered (Si–B–C) ceramic in a complex atmosphere $N_2/O_2/H_2O$, High Temp. Corros. Mater. Chem., accepted for publication.
5. Rebillat, F., Martin, X. and Guette, A., Kinetic oxidation laws of boron carbide in dry and wet environments. In *Proceedings of High Temperature Ceramic Matrix Composites 5 (HTCMC 5)*, ed. M. Singh, R. Kerans, E. Lara-Curzio and R. Naslain. The Am. Ceram. Soc., Westerville, Ohio, USA, 2004, pp. 321–326.
6. Quemard, L., Martin, X., Rebillat, F. and Guette, A., Thermodynamic study of B_2O_3 reactivity in $H_2O_{(g)}N_{2(g)}/O_{2(g)}$ atmospheres at high pressure and high temperature. In *Proceedings of High Temperature Ceramic Matrix Composites 5 (HTCMC 5)*, ed. M. Singh, R. Kerans, E. Lara-Curzio and R. Naslain. The Am. Ceram. Soc., Westerville, Ohio, USA, 2004, pp. 327–332.
7. Farizy, G., Mécanisme de fluage sous air de composites $SiC_f/SiBC_m$ à matrice auto-cicatrisante, Ph.D. Thesis, University of Caen, 2002.
8. Viricelle, J. P., Oxidation behaviour of a multi-layered ceramic matrix composite $(SiC)_f/C/(SiBC)_m$. *Comp. Sci. Technol.*, 2001, **61**, 607–614.
9. Jacobson, N., Farmer, S., Moore, A. and Sayir, H., High temperature oxidation of boron nitride: I, monolithic boron nitride. *J. Am. Ceram. Soc.*, 1999, **82**(2), 393–398.
10. Opila, E. J. and Hann Jr., R. E., Paralinear oxidation of CVD SiC in water vapor. *J. Am. Ceram. Soc.*, 1997, **80**(1), 197–205.
11. Opila, E. J., Oxidation and volatilisation of silica formers in water vapor. *J. Am. Ceram. Soc.*, 2003, **86**(8), 1238–1248.
12. Robinson, R. C. and Smialek, J. L., SiC recession caused by SiO_2 scale volatility under combustion conditions: I, experimental results and empirical model. *J. Am. Ceram. Soc.*, 1999, **82**(7), 1817–1825.
13. Yuri, I., Hisamatsu, T., Etori, Y. and Yamamoto, T., Degradation of silicon carbide in combustion gas flow at high temperature and speed. In *Proceedings of ASME TURBOEXPO 2000*, 2000.
14. Bouillon, E., Abbé, F., Goujard, S., Pestourie, E. and Habarou, G., Mechanical and thermal properties of a self sealing matrix composite and determination of the lifetime duration. *Ceram. Eng. Sci. Proc.*, 2000, **21**(3), 459–467.
15. Bouillon, E., Lamouroux, F., Baroumes, L., Cavalier, J. C., Spriet, P. and Habarou, G., An Improved Long Life Duration CMC for Jet Aircraft Engine Applications, ASME TURBO EXPO 2002, Amsterdam, The Netherlands, 2002, ASME ID GT-2002-30625.
16. Quemard, L., Rebillat, F., Guette, A. and Tawil, H., Development of an original design of high temperature-high pressure furnace. In *Proceedings of High Temperature Ceramic Matrix Composites 5 (HTCMC5)*, ed. M. Singh, R. Kerans, E. Lara-Curzio and R. Naslain. The Am. Ceram. Soc., Westerville, Ohio, USA, 2004, pp. 543–548.
17. Corne, P., Rechiniac, C. and Lamon, J., Approche des propriétés de l'interface fibre-matrice dans les composites à matrice céramiques: résistance à la décohesion. In *Proceedings of JNC 8*, ed. O. Allix, J. P. Favre and P. Ladeveze, 1992, pp. 213–223.
18. Lamon, J., Rebillat, F. and Evans, A., Assessment of a microcomposite test procedure for evaluating constituent properties of ceramic matrix composite. *J. Am. Ceram. Soc.*, 1995, **78**(2), 401–405.
19. Ogbuji, L. U. J. T., A pervasive mode of oxidative degradation in a SiC-SiC composite. *J. Am. Ceram. Soc.*, 1998, **81**(11), 2777–2784.
20. Ogbuji, L. U. J. T., Oxidative pest degradation of Hi-Nicalon/BN/SiC composite as a function of temperature and time in the burner rig. In *Proceedings of 23rd International Cocoa Beach Conference on Advanced Ceramic Composites of Cocoa Beach*, 1999.
21. Yun, H. M., Tensile behavior of as-fabrictaed and burner rig exposed SiC/SiC composites with Hi-Nicalon Type S Fibers. In *Proceedings of 26th International Cocoa Beach Conference on Advanced Ceramic Composites*, 2002.
22. Zawada, L., Richardson, G. and Spriet, P., Ceramic matrix composites for aerospace turbine engine exhaust nozzles. In *Proceedings of High Temperature Ceramic Matrix Composites 5 (HTCMC5)*, ed. M. Singh, R. Kerans, E. Lara-Curzio and R. Naslain. The Am. Ceram. Soc., Westerville, Ohio, USA, 2004, pp. 491–498.
23. Bouillon, E., Spriet, P., Habarou, G. and Arnold, T., Engine Experience and Characterization of Self-sealing Ceramic Matrix Composites for Nozzle Applications in Gas Turbine Engine, Presented at IGTI2003: ASME TURBO EXPO 2003, Atlanta, Georgia, USA, 2003, ASME paper ID GT-2003-38967.